



GENERAL ARTICLE

Germline *PTEN* mutations are associated with a skewed peripheral immune repertoire in humans and mice

Ritika Jaini^{1,3,5}, Matthew G. Loya¹, Alexander T. King¹, Stetson Thacker^{1,3}, Nicholas B. Sarn^{1,4}, Qi Yu¹, George R. Stark^{2,3,4} and Charis Eng^{1,3,4,5,*}

¹Genomic Medicine Institute, Lerner Research Institute, Cleveland Clinic, Cleveland, OH 44195, USA,

²Department of Cancer Biology, Lerner Research Institute, Cleveland Clinic, Cleveland, OH 44195, USA,

³Department of Molecular Medicine, Cleveland Clinic Lerner College of Medicine, Case Western Reserve University, Cleveland, OH 44106, USA, ⁴Department of Genetics and Genome Sciences, Case Western Reserve University School of Medicine, Cleveland, OH 44106, USA and ⁵Germline High Risk Focus Group, CASE Comprehensive Cancer Center, Case Western Reserve University School of Medicine, Cleveland, OH 44106, USA

*To whom correspondence should be addressed at: Genomic Medicine Institute, Lerner Research Institute, Cleveland Clinic, 9500 Euclid Avenue, NE-50, Cleveland, OH 44195, USA. Tel: 216-444-3440; Fax: 216-636-1609; Email: engc@ccf.org

Abstract

Individuals with germline mutations in the gene encoding phosphatase and tensin homolog on chromosome ten (*PTEN*) are diagnosed with *PTEN* hamartoma tumor syndrome (PHTS) and are at high risk for developing breast, thyroid and other cancers and/or autoimmunity or neurodevelopmental issues including autism spectrum disorders. Although well recognized as a tumor suppressor, involvement of *PTEN* mutations in mediating such a diverse range of phenotypes indicates a more central involvement for *PTEN* in immunity than previously recognized. To address this, sequencing of the T-cell receptor variable-region β -chain was performed on peripheral blood from PHTS patients. Based on patient findings, we performed mechanistic studies in two *Pten* knock-in murine models, distinct from each other in cell compartment-specific predominance of *Pten*. We found that *PTEN* mutations in humans and mice are associated with a skewed T- and B-cell gene repertoire, characterized by increased prevalence of high-frequency clones. Immunological characterization showed that *Pten* mutants have increased B-cell proliferation and a proclivity towards increased T-cell reactivity upon Toll-like-receptor stimulation. Furthermore, decreases in nuclear but not cytoplasmic *Pten* levels associated with a reduction in expression of the autoimmune regulator (*Aire*), a critical mediator of central immune tolerance. Mechanistically, we show that nuclear *PTEN* most likely regulates *Aire* expression via its emerging role in splicing regulation. We conclude that germline disruption of *PTEN*, both in human and mouse, results in compromised central immune tolerance processes that may significantly impact individual stress responses and therefore predisposition to autoimmunity and cancer.

Received: March 18, 2020. Revised: May 8, 2020. Accepted: June 11, 2020

© The Author(s) 2020. Published by Oxford University Press. All rights reserved. For Permissions, please email: journals.permissions@oup.com

Introduction

As a well-known tumor suppressor gene, phosphatase and tensin homolog on chromosome *ten* (*PTEN*, OMIM *601728) is frequently somatically mutated in sporadic cancers (1, 2) and mutated in the germline in heritable cancer/overgrowth syndromes (3). It negatively regulates phospho-inositol-3-kinase (PI3K) signaling, critical for cell growth, survival, proliferation and motility (4).

Germline *PTEN* mutations occur in subsets of disparate clinical disorders such as Cowden syndrome (OMIM #158350), Bannayan–Riley–Ruvalcaba syndrome (#158350) and autism spectrum disorder (ASD) with macrocephaly (#605309) (3,5,6). Individuals with germline *PTEN* mutations, irrespective of clinical phenotype, are referred to as having *PTEN* hamartoma tumor syndrome (PHTS; 7), characterized by an increased incidence of breast, thyroid and other cancers, as well as ASD in up to 23% of patients (3,8).

In addition to its well-documented association with cancers and ASD, highly variable and often contradictory autoimmune phenotypes have been reported, both in patients with germline *PTEN* mutations (9,10) and in murine models (9–12). At first puzzling, we and others have also shown increased prevalence of Hashimoto's thyroiditis (RR 14.4 versus 5), lymphoid hyperplasia and inflammation in multiple organs such as the gut, thyroid, adrenal glands and lymphatic tissue in individuals with germline *PTEN* mutations (13, 14).

As a crucial regulator of the AKT/mTOR pathway, *PTEN* involvement in peripheral immune cell proliferation and regulation is expected (10,15,16). The canonical functions of *PTEN* may therefore explain the increased incidence of autoimmunity in individuals with germline *PTEN* mutations. However, the extreme variability of phenotypes observed in PHTS patients, ranging from autoimmunity to benign growths and malignant cancers to the spectrum of autism disorders, indicates a more central involvement of *PTEN* in immunity and inflammation. We therefore hypothesized that *PTEN* dysfunction in PHTS patients may impact critical processes involved in establishment of the immune repertoire, which would affect stress response to physiological insults and in turn determine differential predisposition to cancer, autoimmunity and/or ASD.

To further gain insight into the mechanism by which systemic *Pten* dysfunction observed in PHTS patients may impact immune responses, we used murine models with germline mutations in *Pten* that result in constitutive cytoplasmic or nuclear predominant *Pten* localization. The systemic and constitutive decrease in *Pten* in our models allowed observation of the interplay between multiple cell lineages in peripheral and central immunological sites (in contrast to cell specific *Pten* mutant models), therefore providing a more physiologically relevant assessment of immune parameters observed in patients with germline *PTEN* mutations (11,15).

Results

Germline *PTEN* mutations are associated with increased prevalence of high-frequency T-cell clones in the peripheral immune repertoire

TCRV β repertoires of a selected cohort of *PTEN* mutation-positive individuals were analyzed to interrogate the impact of their germline *PTEN* mutations on peripheral immunity. Our analyses revealed increased prevalence of high-frequency T-cell clones (clones with >4%) in the peripheral blood of PHTS individuals (7/35, Fig. 1A) compared to healthy controls (0/35) from

two publicly available cohorts (immune access data, adaptive biotechnology; Fig. 1B, Supplementary Material, Fig. S1). These analyses reveal that different germline *PTEN* mutations (non-synonymous, nonsense as well as pathogenic/likely pathogenic missense variants) are associated with significant increase in the prevalence of high-frequency T- and B-cell clones in peripheral blood (Fig. 1C). Interestingly, the one variant in the intronic region (benign variant) included in the cohort (c.1026 + 327 > G) and the only one clearly classified as non-pathogenic showed no increase in TCRV β frequencies in any of the individuals with the mutation. All other deletion or missense mutations in exons, where multiple individuals could be sampled, showed presence of high-frequency TCRV β clones in one or more individual.

To assess if a skewed immune repertoire is a common phenomenon observable in other models of systemic *Pten* decrease, we evaluated the peripheral T-cell immune repertoire (*Tcrb* diversity) of *Pten*^{m3m4} mice. Mutant and wild-type mice housed in the same cage for their entire lifetimes were compared. Significantly, more high-frequency T-cell clones (>0.05% in the periphery) were found in *Pten*^{m3m4/m3m4} and *Pten*^{WT/m3m4} mutants compared to wild-type littermates (Fig. 2A). In fact, the top 10 most frequent T-cell clones were exclusively present in *Pten* mutants ($P = 0.014$, Fig. 2A right panel). The presence of a skewed immune repertoire was further reinforced by the greater prevalence of high-frequency B-cell clones in *Pten*^{m3m4/m3m4} compared to *Pten*^{WT/m3m4} and wild-type littermates (Fig. 2B). In contrast to the *Pten*^{m3m4} mutants with reduced nuclear *Pten*, the B6-*Pten*^{WT/Y68H} mice with normal nuclear *Pten* levels showed little to no high-frequency T-cell clones (Fig. 2C), thereby suggesting a unique role for nuclear *Pten* in immune repertoire generation.

Mice with systemically decreased *Pten* expression show predisposition to autoimmunity, T-cell hyper-reactivity and B-cell hyperactivation

100% of *Pten*^{m3m4/m3m4} homozygous mutants ($n > 60$) have an immune activation phenotype, characterized by splenomegaly, thymic hypertrophy and intestinal B-cell hyperplasia, phenotypes similar to those reported in PHTS patients (Supplementary Material, Fig. S2). *Pten*^{WT/m3m4} mice display similar but comparatively moderate phenotypes. Uveitis (approximately 10% of mice) and hemorrhagic lymph nodes (approximately 50% of mice) were also observed but only in *Pten*^{m3m4/m3m4} homozygous mutants.

Further immune characterization revealed significantly increased pro-inflammatory IgG2b antibody in CD1-*Pten*^{m3m4/m3m4} (5-fold increase, $P = 4 \times 10^{-5}$) and CD1-*Pten*^{WT/m3m4} (2-fold increase, $P = 0.049$) mice compared to *Pten*^{WT/WT} littermates (Fig. 3A and B). Circulating antibodies were reactive to IFN- α ($n = 10$, *Pten*^{m3m4/m3m4} versus *Pten*^{WT/WT} $P = 0.0023$, Fig. 3C) similar to reports in other systemic autoimmune diseases. Higher serum IgG levels were associated with increased IgG infiltration in adrenal glands of *Pten*^{m3m4} mutants (Fig. 3D, quantified in Supplementary Material, Fig. S3A left panel). However, no significant antibody infiltration was observed in the heart, liver, lung, thyroid, ovary or testis. Significant B220+ cellular infiltrates were observed in the kidney and liver of *Pten*^{m3m4/m3m4} mice (Supplementary Material, Fig. S2F, quantified in Supplementary Material, Fig. S3A center panel). B-cell germinal center formation in the spleen of *Pten*^{m3m4} mutant mice (Fig. 3E bottom panels) indicated greater B cell activation, typically seen in various systemic rheumatoid and autoimmune diseases. B cell numbers were also increased by approximately

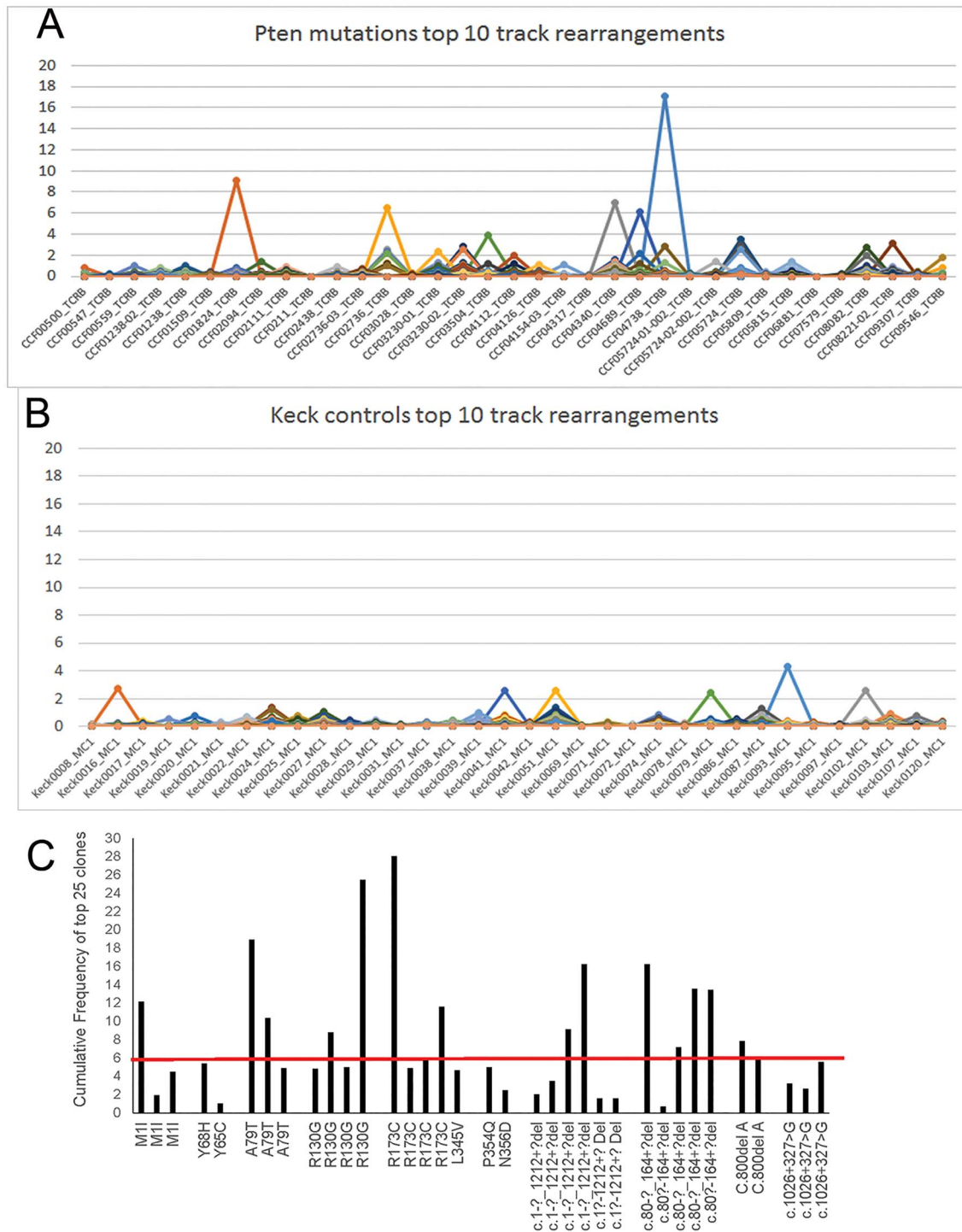


Figure 1. Patients with *PTEN* mutations have a skewed T-cell repertoire with increased prevalence of high-frequency T-cell clones compared to *PTEN* wild-type population. (A) Tracked frequencies of top 10 TCRVB clones in patients with *PTEN* mutations (Cleveland Clinic cohort; $n = 35$) compared to tracked frequencies of top 10 TCRVB clones in publicly available data from healthy controls. (B) Keck cohort controls ($n = 34$) and (Supplementary Material, Fig. S1) HIP cohort controls ($n = 35$). (C) Cumulative frequencies of top 25 clones in PHTS patients identified by their *PTEN* mutation. Red line depicts an arbitrary cut off at 5% cumulative frequency of top 25 clones to highlight propensity towards higher clonal frequencies associated with specific *PTEN* mutations.

3-folds in hypertrophic lymph nodes of *Pten* mutant mice by immunohistochemistry (IHC) (Fig. 3F, Supplementary Material, Fig. S3A right panel) and flow cytometry (19.75% B cells in *Pten*^{m3m4/m3m4} mice >10.4% in *Pten*^{WT/m3m4} mice >7.1% in *Pten*^{WT/WT}; $P = 0.014$; $n = 3$; Fig. 3G). These analyses of both lymphoid and non-lymphoid compartments suggest ongoing B-cell

inflammatory activity in mice with constitutively decreased *Pten*.

CD1-*Pten*^{m3m4} mice showed significantly higher lymph node ELISpot frequencies upon toll-like receptor (TLR) (Fig. 4A left panel) or non-specific T-cell stimulation with Concanavalin A (Fig. 4A right panel, $P = 0.019$). Highest IFN γ responses were

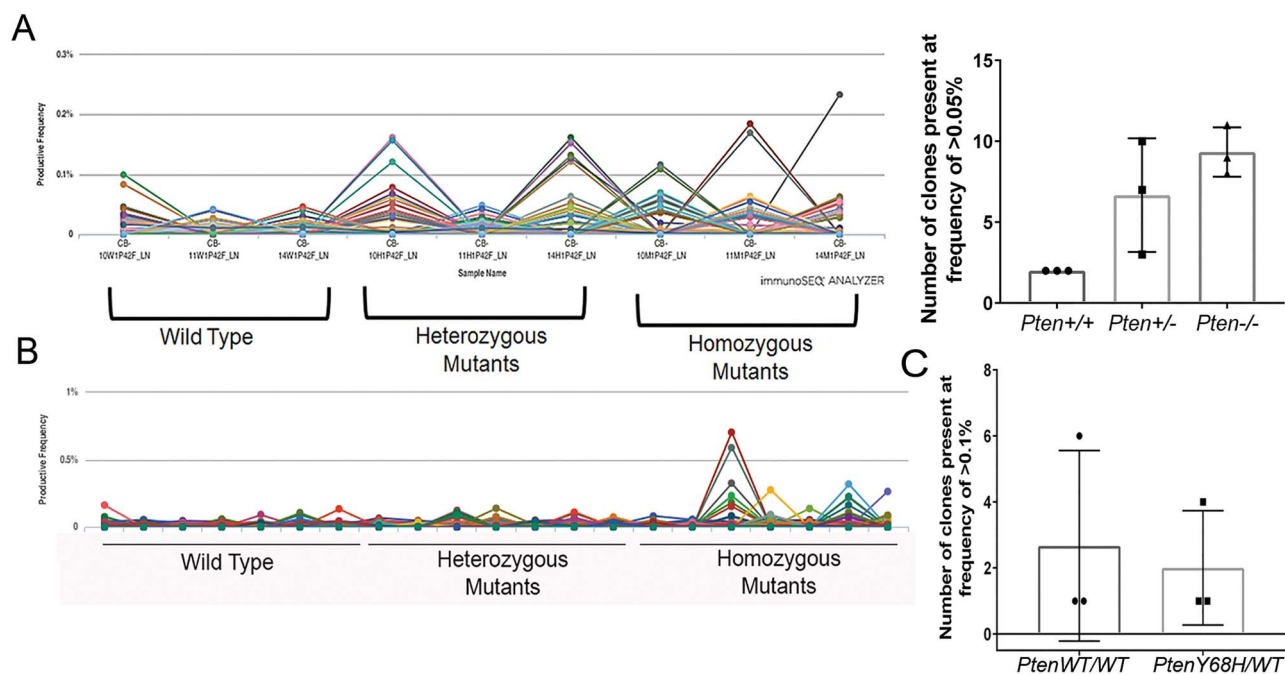


Figure 2. Systemically decreased *Pten* is associated with a skewed peripheral immune repertoire with increased high-frequency clones in mice. *Tcrb* sequencing analysis showing: (A) Left panel: top 10 most frequent *Tcrb* clones in CD1-*Pten*^{m3m4} mice tracked by frequency of occurrence ($n = 9, 3$ for each genotype). Right panel: the number of clones present at >0.05% frequency in CD1 background, homozygous mutant *Pten*^{m3m4/m3m4} (*Pten*^{-/-}) mice compared to *Pten*^{WT/m3m4} heterozygous mutant (*Pten*^{+/-}) and *Pten*^{WT/WT} wild-type (*Pten*^{+/+}) mice ($P = 0.014$). (B) Top 10 most frequent BCR/IgH clones tracked by frequency (Y-axis) of occurrence in all mice tested ($n = 7$ for each genotype). (C) Prevalence of high-frequency clones in *Pten*^{WT/Y68H} mutants and their wild-type (*Pten*^{WT/WT}) littermates.

seen to TLR 7/8 agonists (R848, $P = 0.03$) > TLR9 (CpG, ODN1826, $P = 0.12$) > TLR4 (lipopolysaccharide) stimulation. In contrast to the B-cell expansion demonstrated above, no CD4+ T-cell expansion was observed in naive *Pten* mutants in spite of the increased prevalence of high-frequency T-cell clones ($P = 0.75$, Fig. 4B). In accordance, negligible T-cell infiltration was observed in peripheral organs (data not shown). Also, no major differences in T-regulatory cell frequencies were observed among the three *Pten* genotypes (4.5% in *Pten*^{WT/WT} versus 4.8% in *Pten*^{WT/m3m4} versus 4.2% in *Pten*^{m3m4/m3m4}, Fig. 4C). Similar pro-inflammatory T-cell reactivity was observed in the B6-*Pten*^{WT/m3m4} (Fig. 4D) as well as *Pten*^{Y68H/WT} mice with systemic *Pten* decrease, albeit with overall lower frequencies compared to *Pten*^{m3m4/WT} at 6 weeks of age (Fig. 4E). Collectively, our data suggest a proclivity for pro-inflammatory Th1 responses in systemic *Pten* mutants upon perception of danger signals but no ongoing pathogenic T-cell expansion or T-regulatory cell defects in naive unchallenged mice.

Reduced nuclear *Pten* expression is associated with decreased expression of the autoimmune regulator Aire in mTECs

Since central T-cell repertoire selection is mediated by the medullary thymic epithelial cells (mTECs), we compared the thymus of *Pten* mutant versus wild-type littermates. Interestingly, *Pten* was found to be predominantly expressed in the thymic medulla, where mTECs are known to reside. More importantly, we observed a significant decrease in *Pten* expression in the medulla of *Pten* mutants compared to wild-type (Supplementary Material, Fig. S4A). This led us to interrogate if there were any functional changes in mTECs as a result of decreased *Pten* expression. The autoimmune regulator (AIRE) is a key transcription factor specifically expressed in mTECs. AIRE

expression allows deletion of T-cells with high T-cell receptor affinity against self-proteins (17). We observed a significant decrease in Aire expression at P24 and P42 in the thymus of CD1-*Pten*^{m3m4/m3m4} < *Pten*^{WT/m3m4} < *Pten*^{WT/WT} by IHC (Fig. 5A, middle and bottom rows, quantified in Supplementary Material, Fig. S3B), confocal microscopy (Supplementary Material, Fig. S4B, integrated density 29.01 versus 8.28) and Western blotting (Supplementary Material, Fig. S4C). Since endogenous Aire is expressed at very low levels in <1% of the thymic cell population, we immunoprecipitated it specifically from whole thymic lysates and confirmed its decrease in *Pten*^{m3m4/m3m4} mice (Supplementary Material, Fig. S4D). A significant decrease in Aire expression was also evident in the lymph nodes of *Pten*^{m3m4/m3m4} mice (Fig. 5B). B6-*Pten*^{WT/m3m4} also showed lower thymic Aire expression (Fig. 5C, Supplementary Material, Fig. S3B). More importantly, the median fluorescence intensity of Aire within the mature MHC-II^{hi}-CD80^{hi} mTEC population was lower in the *Pten*^{m3m4/m3m4} mice compared to wild-type (median fluorescence intensity (MFI) of 68 744 versus 82 386; % decrease of 16.5%), indicating decreased Aire expression per cell ($n = 10$, Fig. 5D and Supplementary Material, Fig. S4F). No significant differences were observed in the proportions of MHC-II^{lo}-CD80^{lo} (immature mTECs, 26.5% *Pten*^{WT/WT} versus 19.4% *Pten*^{WT/m3m4} versus 32.9% *Pten*^{m3m4/m3m4}) and MHC-II^{hi}-CD80^{hi} (mature mTECs, 27.85% *Pten*^{WT/WT} versus 36.5% *Pten*^{WT/m3m4} versus 35.3% *Pten*^{m3m4/m3m4}) cells in mutant versus wild-type mice (Supplementary Material, Fig. S4E). In contrast, *Pten*^{WT/Y68H} mutant mice with nuclear-predominant *Pten* expression showed similar Aire expression to their wild-type littermates (Fig. 5E, Supplementary Material, Fig. S3B). These data comparing three systemic *Pten* mutant mouse models characterized by distinct cell compartmentalization of *Pten* collectively show that a decrease in nuclear *Pten* but not of cytoplasmic *Pten* results in reduced Aire expression in the thymus as well as lymph nodes.

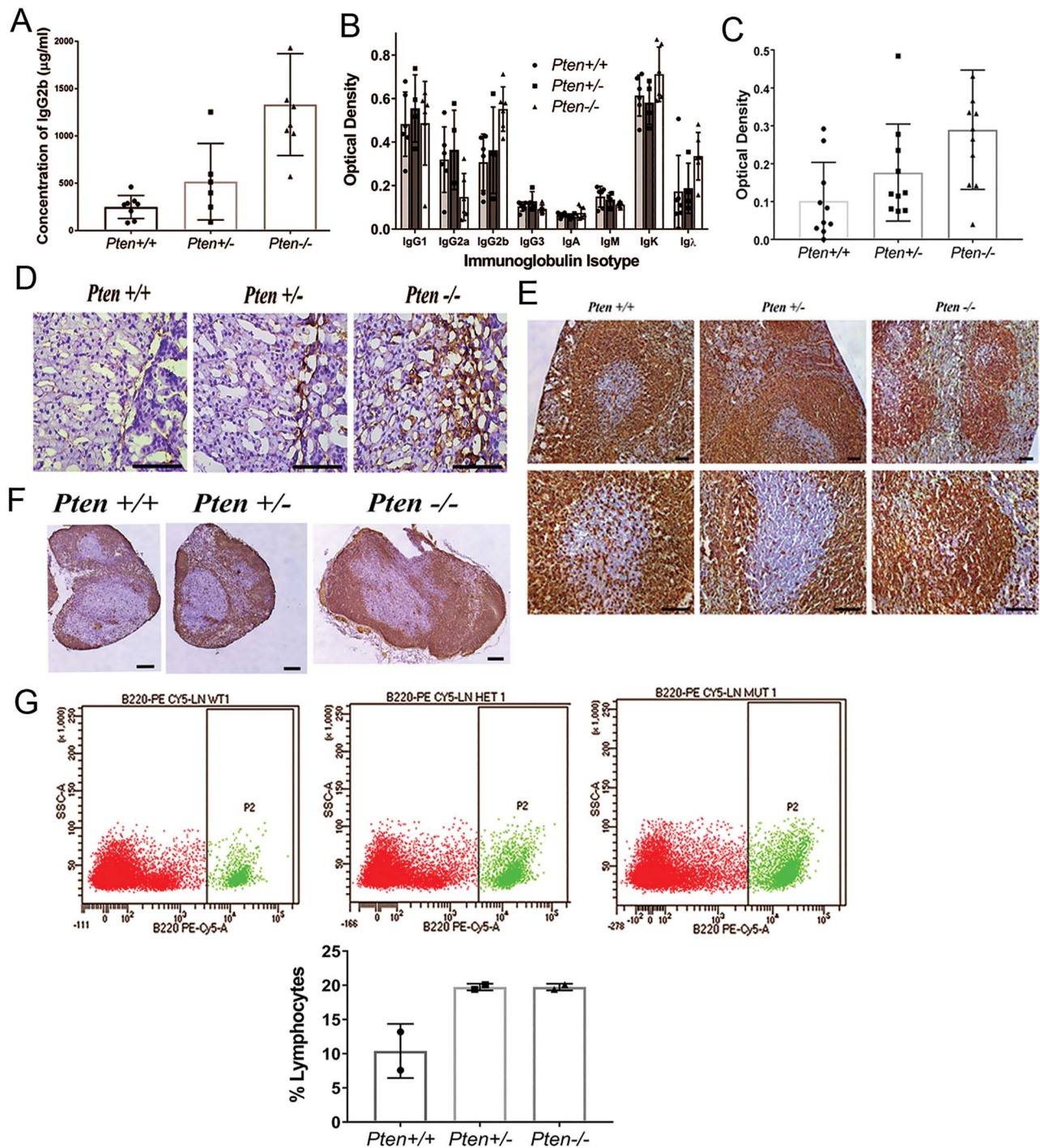


Figure 3. Systemic and constitutive decrease in Pten expression is associated with B-cell hyperactivation. (A) Enzyme-linked immunosorbent assay (ELISA) quantification for serum IgG2b in CD1-*Pten*^{m3m4/m3m4} (▲ *Pten*^{-/-}; $P = 4 \times 10^{-5}$; $n = 8$) and CD1-*Pten*^{m3m4/WT} (■ *Pten*^{+/-}; $P = 0.049$; $n = 6$) mice compared to CD1-*Pten*^{WT/WT} litter mates (● *Pten*^{+/+}; $n = 8$). (B) Isotyping of serum Immunoglobulin in CD1-*Pten*^{m3m4} mice. (C) ELISA quantifying IFN- α reactive antibodies in sera of CD1-*Pten*^{m3m4} mice ($n = 10$; $P = 0.0023$). (D) Representative IHC showing IgG infiltration in adrenal glands of CD1-*Pten*^{m3m4} mice. (E) IHC for B220+ cells showing germinal center formation in the spleen in CD1-*Pten*^{m3m4/m3m4} (*Pten*^{-/-}) mice. (F) IHC for B220+ cells in lymph nodes of CD1-*Pten*^{m3m4} mutant mice, also showing lymph node hypertrophy. Quantification of IHC in Supplementary Material, Fig. S3A. Scale bar = 100 μ m. (G) Top panel: representative flow cytometry plots showing frequency of B-cell in lymph nodes of CD1-*Pten*^{m3m4} mice; Bottom panel: graphical summary of mean B-cell frequencies in CD1-*Pten*^{m3m4} mice ($n = 3$ experiments; $P = 0.014$).

To evaluate if the reduction in Aire expression in *Pten* mutants was functionally relevant, we analyzed the Aire-dependent expression of tissue-specific antigens (TSAs) in the thymus. Since single time-point TSA expression can be a highly variable transcriptional snapshot in time, we conducted a time course

analysis for Insulin2 expression, which showed continued low expression in *Pten*^{m3m4/m3m4} mutants throughout all ages (Fig. 5F). Collectively, our data suggest that *Pten* mutants have a loss in Aire expression with functionally relevant consequences on the central tolerance and immune repertoire selection machinery.

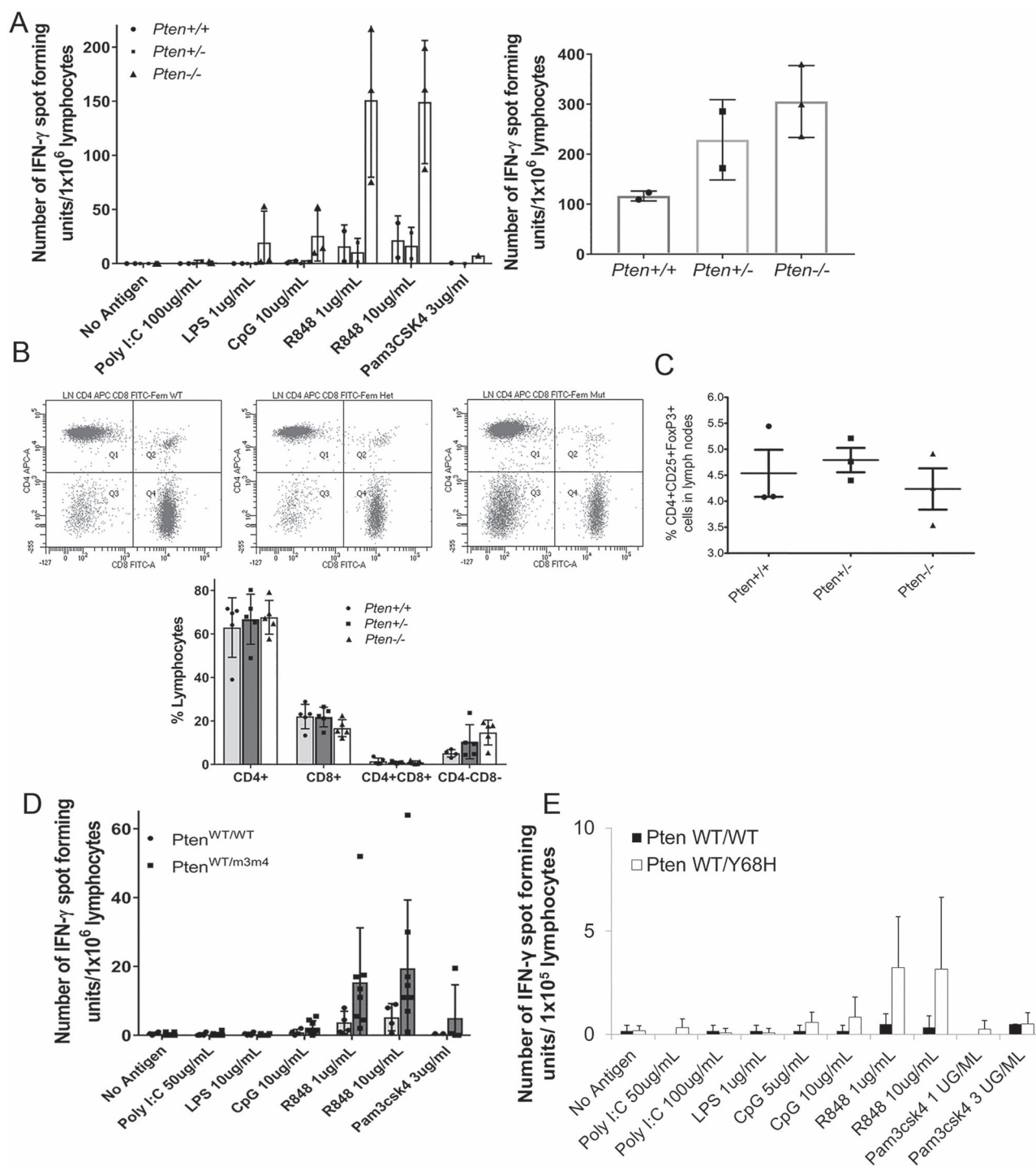


Figure 4. Mutants with systemically decreased Pten levels have a predisposition for T-cell hyper-responsiveness. (A) EliSpot frequencies of IFN γ -producing lymph nodes cells in *Pten*^{m3m4} mice after TLR stimulation (left panel, n = 3, R848 $P = 0.03$, CpG $P = 0.12$) and non-specific stimulation of T-cells with Concanavalin A (right panel, n = 3, $P = 0.019$). (B) Top panel: representative flow cytometry plots (n = 5 experiments) showing frequencies of T-cell subsets in lymph nodes of CD1-*Pten*^{m3m4} mice. Bottom panel: graphical summary showing mean frequencies of CD4+ ($P = 0.75$ *Pten*^{-/-} compared to WT), CD8+ ($P = 0.0047$ *Pten*^{-/-} compared to WT) and CD4-CD8- ($P = 0.032$ *Pten*^{-/-} compared to WT) T-cells. (C) Flow cytometry-based mean frequencies of T-regulatory cells in lymph nodes of CD1-*Pten*^{m3m4} mice (n = 3; P -value = not significant). Error bars depict standard deviation. (D, E) EliSpot frequencies of IFN γ producing T-cells in response to TLR stimulation in (D) B6-*Pten*^{WT/m3m4} and (E) *Pten*^{WT/Y68H} lymph nodes.

Nuclear Pten regulates expression and splicing of the Aire transcript

To address the mechanism by which nuclear Pten may mediate a decrease in Aire protein expression, we quantified Aire transcript levels in the thymus throughout development. As expected, WT

thymi showed high levels of Aire transcript during early postnatal stages that declined with age. However, Aire mRNA transcript levels in *Pten*^{m3m4/m3m4} mice remained low at early postnatal stages and throughout development (P2, $P = 0.009$, and P8, $P = 0.4$, Fig. 6A).

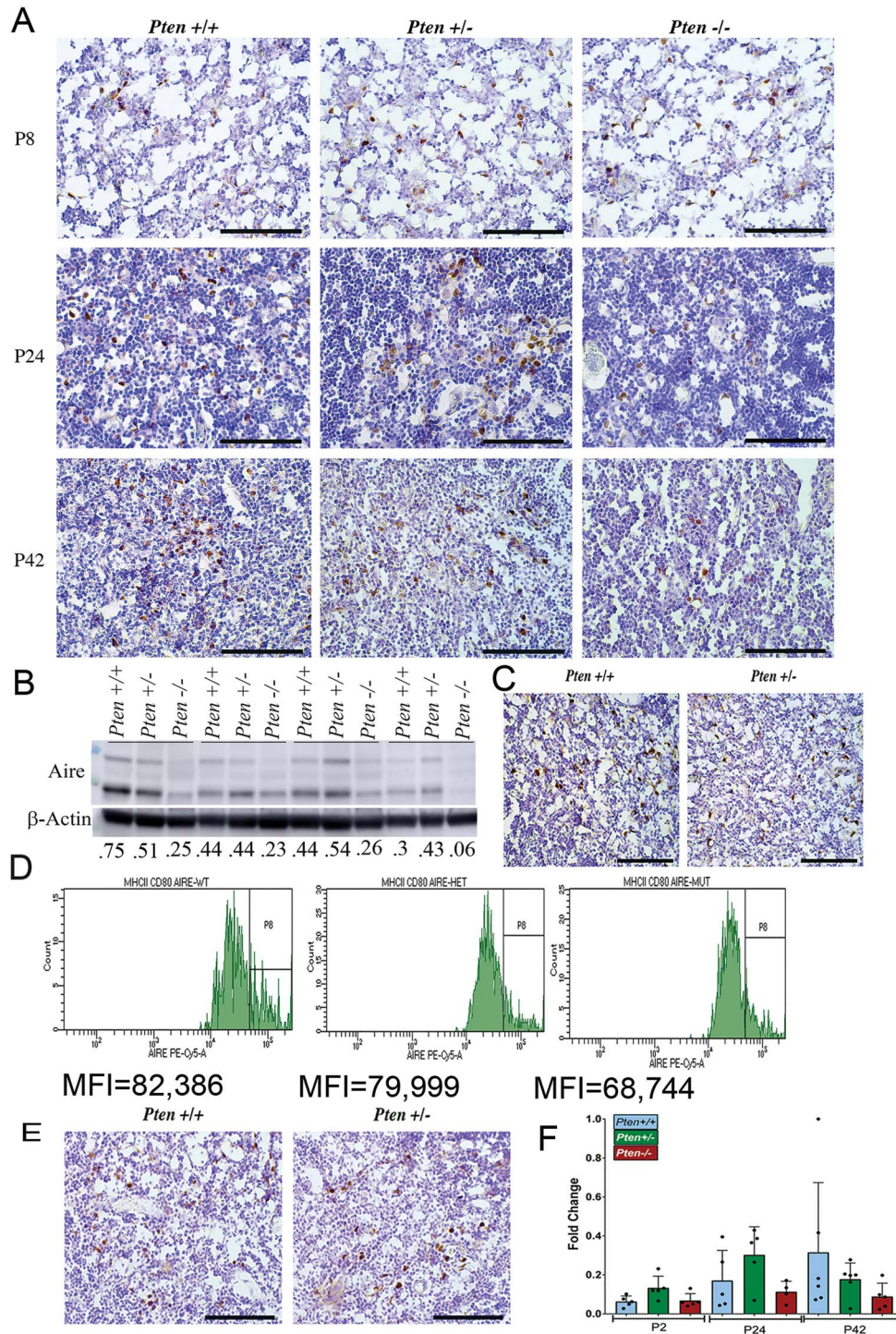


Figure 5. Decreased nuclear Pten expression is associated with significantly reduced expression of the autoimmune regulator Aire. (A) Representative ($n = 3$) IHC for Aire expression (brown DAB staining) in the thymus of CD1-*Pten*^{m3m4} at P8 (top row), P24 (middle row) and P42 (bottom row). (B) Western blot for Aire expression in lymph nodes of CD1-*Pten*^{m3m4} mice ($n = 4$ each genotype). Numbers below the figure are ratios of Pten/ β -Actin band intensities. (C) Representative IHC for Aire expression (brown nuclear DAB staining) in thymi of B6-*Pten*^{m3m4} mice at 6 weeks of age ($n = 3$ mice). (D) Flow cytometry histograms showing MFI of Aire expression in the mature mTEC population (16.5% decrease in *Pten*^{-/-} mutants compared to *Pten*^{+/+}, $n = 10$ mice pooled for each genotype). (E) Representative IHC for Aire expression (brown nuclear DAB staining) in thymi of B6-*Pten*^{Y68H} mice with predominantly nuclear Pten, at 6 weeks of age ($n = 4$ mice). (F) Time course of q-RT-PCR-based relative expression of Insulin 2 in thymus at different ages. Quantifications of IHC in Supplementary Material, Fig. S3B. Error bars depict standard deviation. Scale bar = 100 μ m.

Recent studies have highlighted the post-transcriptional regulation of Aire by alternative splicing, specifically intron retention (18). Also, decreased expression of the lysyl hydroxylase

Jmjd6 has been implicated in increased retention of Aire intron-2 (19). An increase in the ratio of intron-2 retaining transcripts to mature Aire transcripts ($P = 0.036$, Fig. 6B) and

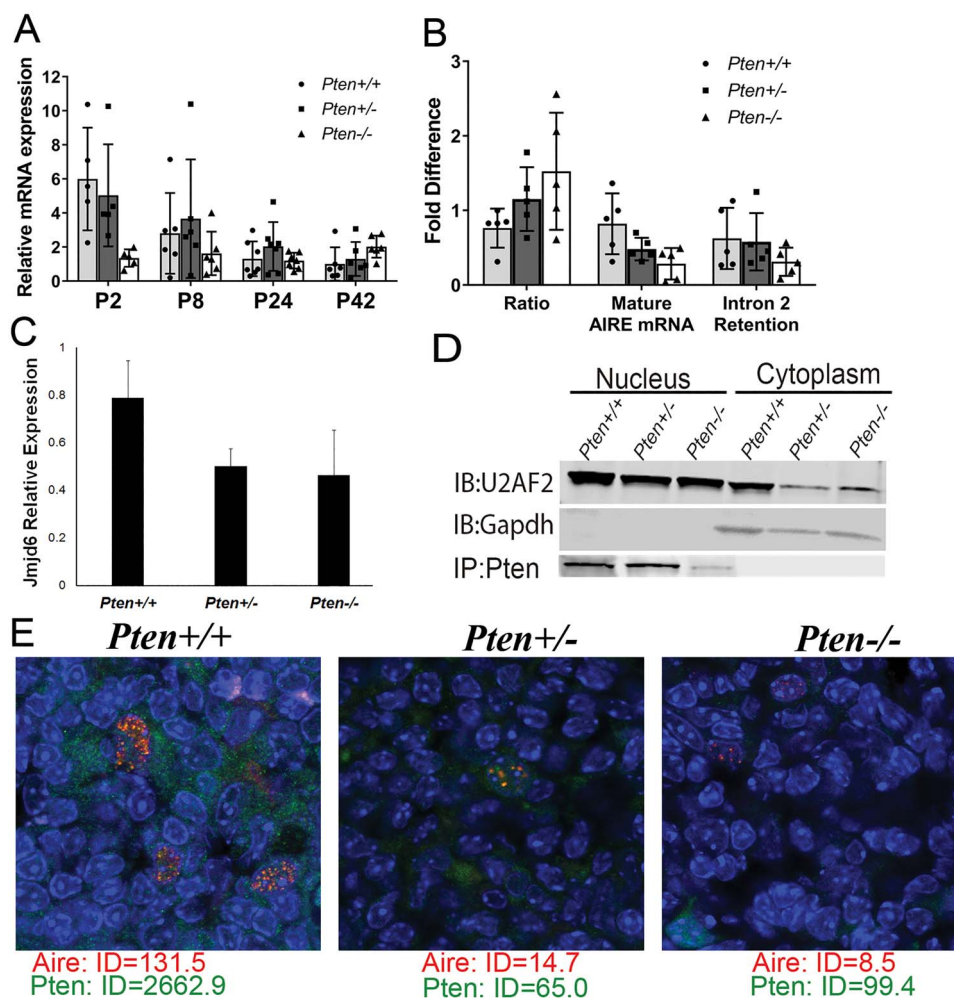


Figure 6. Nuclear Pten regulates expression and splicing of the Aire transcript. (A) qRT-PCR-based fold difference in Aire mRNA transcript levels at different stages of postnatal development in CD1-*Pten*^{m3m4} mice (P2, $P = 0.009$, and P8, $P = 0.4$; $n = 6$). (B) qRT-PCR-based fold difference in intron-2 retaining versus mature Aire transcript in mice with reduced nuclear Pten ($n = 5$, $P = 0.036$). (C) q-RT-PCR for relative Jmjd6 expression in thymus of CD1-*Pten*^{m3m4} mice (representative of three separate experiments with different primer sets, $n = 5$ per experiment, $P = 0.018$). (D) Immunoblots ($n = 2$ experiments) on nuclear and cytoplasmic fractions of CD1-*Pten*^{m3m4} thymus showing total levels of U2af2 (top panel) and U2af2 bound to immunoprecipitated Pten (bottom panel). (E) Confocal imaging showing co-localization (yellow overlay) of Aire protein (red) with Pten protein (green) only in the nucleus (blue) of CD1-*Pten*^{m3m4} mTECs at 6 weeks of age. Integrated density of Aire and Pten stain is shown below each respective panel. Error bars depict standard deviations.

decreased expression of Jmjd6 ($P = 0.018$, Fig. 6C) was observed in *Pten*^{m3m4/m3m4} mutant thymus. Total levels of U2 small nuclear ribonucleoprotein auxiliary factor 65-kD subunit (U2AF65 or U2AF2), a known substrate of Jmjd6, were not different in the nucleus of WT and *Pten*^{m3m4} mutant thymi. However, U2af2 binding to nuclear Pten was significantly reduced in the *Pten*^{m3m4} mutant thymus (Fig. 6D). These data suggest reduced recruitment of U2af2 to the likely Pten-U2af2-Jmjd6 interaction within the spliceosome in Pten mutants leading to alternative splicing and expression of Aire. Interestingly, Pten (green) and Aire (red) proteins were observed to co-localize (yellow overlay) in the nucleus (blue) of mTECs (Fig. 6E). This observed protein-protein interaction between nuclear Pten and Aire may indicate additional regulatory interactions between the two proteins that should be explored as part of future studies.

Discussion

We show that a systemic reduction in nuclear PTEN results in a skewed peripheral immune repertoire with significantly

increased prevalence of high-frequency T- and B-cell clones in PHTS patients. This observation was found to be true also in murine models with systemic Pten mutations. This is likely the result of a more central involvement of PTEN in T-cell repertoire selection than previously appreciated. Altered immune repertoire composition in patients with germline PTEN mutations may have significant consequences on individual responses to physiological stress, which in turn would modulate individual susceptibility to cancer, autoimmunity and/or neurodevelopmental disorders like ASD (9–14).

The AIRE is a key central regulator, critical for immune repertoire determination. As a transcription factor expressed by specialized mTECs, AIRE facilitates expression of an ‘immunological self-shadow’ during T-cell negative selection, thus playing an essential role in deletion of self-reactive clones and development of the T-cell repertoire (17). Germline mutations in the AIRE gene lead to a systemic autoimmune disease, autoimmune polyendocrinopathy-candidiasis-ectodermal dystrophy, indicating the importance of AIRE in controlling autoimmunity (20). It is interesting that AIRE as a transcription factor allows expression

of 'self-proteins' by chromatin de-condensation (21), whereas nuclear PTEN is known to be a regulator of genomic integrity and chromatin stability (22,23). Although various signaling mediators such as the Rb and TNF family members as well as Pten have been shown to affect thymic development and mTEC maturation (24,25), no direct transcriptional regulatory association between PTEN, a master regulator of cellular proliferation, and AIRE, a key regulator of immunity, has been established until now.

In light of the previously established roles of PTEN in adaptive immunity and immune function (26), the prevalence of high-frequency clones in the peripheral immune repertoire of naïve unchallenged systemic/germline mutants (PHTS patients or *Pten*^{m3m4} mice) may be a combined effect of both escaped high-frequency clones resulting from reduction in thymic Aire expression and their subsequent clonal expansion fueled by Pten mutation-mediated increase in PI3K signaling and proliferation in peripheral immune cells. The increase in high-frequency clones in *Pten*^{m3m4} mutants was reflected only as a minor increase in CD4+ T-cell numbers, since high-frequency clones comprise less than 1% of the T-cell repertoire in a naïve system. However, such a potentially self-reactive system would remain predisposed to significantly increased CD4+ T-cell help and B-cell proliferation upon receipt of stress signals, resulting in acute or chronic inflammation. The nature of the environmental stressors encountered (gene–environment interaction) would likely influence an individual's phenotypic outcome ranging from the spectrum of ASD to autoimmunity to cancer. Monitoring of TCRVB frequencies would probably correlate with disease onset or progression in predisposed individuals even with the same PTEN variant. Larger sample size studies are needed to determine the penetrance of specific PTEN variation in affecting TCRVB repertoire changes. The overall impact on the immune repertoire of escaped high-frequency clones from the thymus versus peripheral T- and B-cell expansion cannot be separated in animal models of systemic Pten decrease. However, the systemic and constitutive nature of Pten mutations in our models was a critical feature that allowed us to observe the decrease in Aire expression instead of masking it with deleterious effects on thymic development as is seen in cell-specific Pten mutant models (27).

The cytoplasmic role of PTEN as a regulator of the PI3K-AKT signaling pathway has been well established (4). However, its importance as a nuclear regulator of genomic integrity and transcription is emerging (22,23,28,29). We propose an additional role for nuclear Pten in regulating Aire expression via splicing mechanisms. Although we show predisposition to higher peripheral T-cell reactivity in both the *Pten*^{m3m4} and *Pten*^{Y68H} mutants, due to systemic loss of total Pten, only the *Pten*^{m3m4} mutants showed increased high-frequency T-cell clones in the periphery. We recognize that the cell compartment-specific murine models compared here result from mutations in distinct regions of the Pten molecule and therefore, different Pten functionality is implicated. However, both mutations result in hyper-phosphorylation of Akt as expected (data not shown). The *Pten*^{Y68H} mutation maps to the phosphatase domain and therefore is considered more functionally deleterious. However, only the *Pten*^{m3m4} mutation in the C2 domain that induces predominantly cytoplasmic expression of the protein resulted in a significant impact on Aire expression. These observations further support that the reduction in Aire expression likely is a result of decreased nuclear functions of Pten.

The involvement of Pten in regulation of splicing factors such as U2af2 has been documented (30,31). This interaction could possibly also involve other as yet unidentified splicing factors.

U2af2 is a known substrate for Jmjd6, a nuclear protein that catalyzes lysyl hydroxylation of splicing regulators (32,33). As a widely involved splicing factor, U2AF2 has been shown to co-immunoprecipitate with JMJD6 as well as PTEN (31,33). Recently, deficiency of Jmjd6 has been implicated in increased retention of intron-2 of Aire (18), whereby introduction of a premature termination codon at the N-terminus of the Aire transcript results in truncated Aire protein. Increased proportions of immature/truncated Aire protein also cause mislocalization of the mature/full length Aire protein to the cytoplasm instead of the nucleus, causing accelerated degradation of both the truncated and mature proteins (18,19). Interestingly, our confocal imaging data also show co-localization of Pten and Aire within the nucleus. Our data suggest reduced recruitment of U2af2 to the likely Pten–U2af2–Jmjd6 interaction within the spliceosome in Pten mutants leading to alternative splicing and expression of Aire, and possibly of a wide range of other transcripts. Therefore, multifactorial mechanisms are implicated in Pten-mediated regulation of Aire expression, probably involving transcriptional control, defective recruitment of U2af2 to the spliceosome and transcript/protein stability. These observations warrant more detailed mechanistic investigations. Overall, our finding that Pten modulates immune repertoire composition expands the involvement of Pten in central immunity and establishes it as an important underlying factor for individual predisposition to chronic inflammation and differential susceptibility to cancer, autoimmunity or aberrant neurodevelopment. Immune repertoire monitoring and potentially modulation in at-risk individuals with germline mutations in PTEN may provide predictive benefit for disease management.

Material and Methods

Murine models

CD1 and C57Bl/6 mice were commercially procured (Jackson Labs, Bar Harbor, MI). *Pten*^{m3m4} mutants on CD1 (*CD1-Pten*^{m3m4/m3m4}, denoted as *Pten*^{−/−}) and C57Bl/6 (*B6-Pten*^{m3m4}) backgrounds and *Pten*^{Y68H} mutants were generated as described previously (34–36). *Pten*^{m3m4/m3m4} and *Pten*^{WT/m3m4} germline mutants are characterized by significantly reduced nuclear Pten expression, compared to wild-type (*CD1-Pten*^{WT/WT}, denoted as *Pten*^{+/+}). In contrast, *Pten*^{Y68H} mutants have predominantly nuclear Pten expression. Both models show a constitutive decrease in total Pten protein (34–36). Age- and sex-matched *Pten* wild-type littermates were used as controls.

Animal ethics statement. All procedures were approved by the Cleveland Clinic's Institutional Animal Care and Use Committee under protocol numbers 2018-1952 and 2017-1879 and guided by the Principles of Laboratory Animal Care formulated by the National Society for Medical Research.

Human subjects

Peripheral blood DNA samples were procured from patients that presented at the Cleveland Clinic Center for Personalized Health with disease symptoms that warranted PTEN mutation testing. PTEN mutations were identified by routine Sanger sequencing screening. The selected cohort had an equal distribution of males and females. All selected patients had detailed documentation of immune phenotypes and diagnosis of either ASD or cancers associated with PHTS.

Human subject ethics statement. All human subject accrual and studies were conducted in accordance with the Declaration of Helsinki. All study protocols were approved by the institutional

review board (IRB) of the Cleveland Clinic and conducted under IRB# 8458. Informed consent was obtained from all enrolled subjects.

Immunohistochemistry

IHC staining was performed as previously described for paraformaldehyde fixed, frozen sections (34). Primary antibodies were acquired commercially (supplementary material). Images were acquired on a Leica DM2000 LED microscope using a DFC450C camera and ImageQ Software. Fluorescent confocal images were acquired on a Leica multi-photon confocal microscope at 630× with 3× digital zoom. Digital image analysis was performed using ImageJ (v1.52k; National Institutes of Health, Bethesda, MD). DAB was separated from hematoxylin via an ImageJ plugin (<https://beardatashare.bham.ac.uk/dl/fiGsh6znHZG4BvQ84YSetim/colourdeconvolution.zip>) (37). Images were set to the same standard pixel range background threshold. Mean gray output was converted to optical density (OD) using: $OD = \log [255/\text{mean gray value}]$ (38). Integrated density was calculated as OD × area. Means of integrated density derived from three replicates were graphed.

Enzyme-linked immunosorbent assay

Immunoglobulin isotyping, IgG2b quantifications and anti TNF- α antibodies were tested on sera from six-week-old mice according to manufacturer instructions (eBioscience, San Diego, CA). Antibody pairs were purchased commercially (supplementary material). Serum samples were diluted to 1:10000 in Assay Buffer. Absorbance was measured at 490 nm on a SynergyMx Microplate reader (BioTek, Winooski, VT).

ELISpot

Capture and detection antibody pairs were commercially procured (supplementary material). A total of 1×10^5 lymph node cells or 2×10^5 splenocytes/well were cultured in antibody pre-coated ELISpot plates (Millipore Billerica, MA) and stimulated with specific TLR agonists (InvivoGen San Diego, CA) for 24 hours. ELISpot assays were conducted per antibody manufacturer's instruction (eBioscience). Spots were counted on a CTL S6 Universal V ELISPOT reader and analyzed using the ImmunoSpot 5.1 software (Cellular Technologies, Cleveland, OH).

Flow cytometry

Thymi from ~10 mice were pooled and mechanically dispersed. Tissue was digested with 0.125% (w/v) Collagenase and Dispase cocktail+50KU/ml DNAase for 15 min at 37°C. Cells were resuspended in FACS buffer (5 mM EDTA + 1% fetal calf serum + 0.02% sodium azide in PBS) and incubated for 10 min at 4°C to disrupt rosette formation. A total of 1×10^6 cells were blocked for Fc γ R and surface stained. T-regulatory cell and intracellular Aire staining were performed using the eBioscience™ T-regulatory cell staining kit. Gating strategy for detection of Aire expression in mature mTECs is shown in [Supplementary Material, Fig. S4F](#). Cells were acquired on a Becton Dickinson Fortessa LSR Flow Cytometer and analyzed using BD FACS Diva v.8.0.1 and Flow Jo software v.10.0.7.

Quantitative reverse transcription–polymerase chain reaction

RNA was extracted using the standard Ribozol RNA extraction protocol (VWR Amresco, Solon, OH). Reverse transcription was

performed using the Superscript III First strand synthesis kit. SYBR Green quantitative reverse transcription–polymerase chain reaction (qRT-PCR) was performed using commercially available primers (Genecopoeia, Rockville, MD). Intron-2 retention qRT-PCR was performed using Taqman custom designed primers and probes (supplementary material). Jmjd6 qRT-PCR was performed using three sets of in-house designed primers (Life Technologies, Carlsbad, CA).

Western blotting

A total of 40 μ g total protein lysate in mammalian protein extraction reagent was transferred to a PVDF membrane. Antibodies and reagents were used as detailed in supplementary material. Intensity of bands was quantified using Image Studio Lite v 5.2 software (LI-COR Biotechnology, Lincoln, NE) and normalized to Gapdh/Actin.

Immunoprecipitation

Frozen tissues were lysed in RIPA buffer (50 mM Tris-HCL C₄H₁₁NO₃, 1% NP-40, 0.1% SDS NaC₁₂H₂₅SO₄, 1 mM EDTA C₁₀H₁₆N₂O₈, 250 mM NaCl) and protein concentration set to 2 mg/ml. Aire protein was immunoprecipitated using Protein A/G beads as per manufacturer's instructions (Thermo Scientific, Waltham, MA).

T-cell receptor/B-cell receptor sequencing

DNA was extracted from murine lymph nodes or peripheral blood of PHTS patients using the DNeasy Blood and Tissue Kit (Qiagen, Germantown, MD). Deep sequencing was performed for T-cell receptor variable-region β -chain (TCRVb) diversity analysis. BCR sequencing was performed at survey level on an Illumina platform (Adaptive Biotechnologies Seattle, WA). Sequencing data were analyzed in-house using the ImmunoSeq Analyzer 3.0 software and publicly available healthy control TCRVb data panels (Adaptive Biotechnologies).

Statistical analyses

Statistical significance was determined by performing the two-tailed Student's t-tests on all control and test data. Significance was determined at *P*-values of <0.05.

Supplementary Material

[Supplementary Material](#) is available at HMG online.

Acknowledgements

The authors would like to thank Hannah J. Chen for technical assistance with Aire transcript assays. DNA from peripheral blood of PHTS patients was acquired from the Cleveland Clinic Genomic Medicine Biorepository. C.E. is the Sondra J. and Stephen R. Hardis Endowed Chair of Cancer Genomic Medicine at the Cleveland Clinic and an ACS Clinical Research Professor.

Conflict of Interest statement. None declared.

Funding

Zacconi Program of PTEN Research Excellence; the Ambrose Monell Foundation; National Cancer Institute (P01CA124570; all to C.E.).

References

- Li, J., Yen, C., Liaw, D., Podsypanina, K., Bose, S., Wang, S.I., Puc, J., Miliareis, C., Rodgers, L., McCombie, R. et al. (1997) PTEN, a putative protein tyrosine phosphatase gene mutated in human brain, breast, and prostate cancer. *Science*, **275**, 1943–1947.
- Steck, P.A., Pershouse, M.A., Jasser, S.A., Yung, W.K., Lin, H., Ligon, A.H., Langford, L.A., Baumgard, M.L., Hattier, T., Davis, T. et al. (1997) Identification of a candidate tumour suppressor gene, MMAC1, at chromosome 10q23.3 that is mutated in multiple advanced cancers. *Nat. Genet.*, **15**, 356–362.
- Liaw, D., Marsh, D.J., Li, J., Dahia, P.L., Wang, S.I., Zheng, Z., Bose, S., Call, K.M., Tsou, H.C., Peacocke, M. et al. (1997) Germline mutations of the PTEN gene in Cowden disease, an inherited breast and thyroid cancer syndrome. *Nat. Genet.*, **16**, 64–67.
- Maehama, T. and Dixon, J.E. (1998) The tumor suppressor, PTEN/MMAC1, dephosphorylates the lipid second messenger, phosphatidylinositol 3,4,5-trisphosphate. *J. Biol. Chem.*, **273**, 13375–13378.
- Hobert, J.A., Embacher, R., Mester, J.L., Frazier, T.W. and Eng, C. (2014) Biochemical screening and PTEN mutation analysis in individuals with autism spectrum disorders and macrocephaly. *Eur. J. Hum. Genet.*, **22**, 273–276.
- Zhou, X.-P., Waite, K.A., Pilarski, R., Hampel, H., Fernandez, M.J., Bos, C., Dasouki, M., Feldman, G.L., Greenberg, L.A., Ivanovich, J. et al. (2003) Germline PTEN promoter mutations and deletions in Cowden/Bannayan–Riley–Ruvalcaba syndrome result in aberrant PTEN protein and dysregulation of the phosphoinositol-3-kinase/Akt pathway. *Am. J. Hum. Genet.*, **73**, 404–411.
- Marsh, D.J., Kum, J.B., Lunetta, K.L., Bennett, M.J., Gorlin, R.J., Ahmed, S.F., Bodurtha, J., Crowe, C., Curtis, M.A., Dasouki, M. et al. (1999) PTEN mutation spectrum and genotype-phenotype correlations in Bannayan–Riley–Ruvalcaba syndrome suggest a single entity with Cowden syndrome. *Hum. Mol. Genet.*, **8**, 1461–1472.
- Tan, M.-H., Mester, J., Peterson, C., Yang, Y., Chen, J.-L., Rybicki, L.A., Milas, K., Pederson, H., Remzi, B., Orloff, M.S. et al. (2011) A clinical scoring system for selection of patients for PTEN mutation testing is proposed on the basis of a prospective study of 3042 probands. *Am. J. Hum. Genet.*, **88**, 42–56.
- Tsujita, Y., Mitsui-Sekinaka, K., Imai, K., Yeh, T.-W., Mitsuiki, N., Asano, T., Ohnishi, H., Kato, Z., Sekinaka, Y., Zaha, K. et al. (2016) Phosphatase and tensin homolog (PTEN) mutation can cause activated phosphatidylinositol 3-kinase δ syndrome-like immunodeficiency. *J. Allergy Clin. Immunol.*, **138**, 1672–1680.e10.
- Chen, H.H., Händel, N., Ngeow, J., Muller, J., Hühn, M., Yang, H.-T., Heindl, M., Berbers, R.-M., Hegazy, A.N., Kionke, J. et al. (2017) Immune dysregulation in patients with PTEN hamartoma tumor syndrome: analysis of FOXP3 regulatory T cells. *J. Allergy Clin. Immunol.*, **139**, 607–620.e15.
- Suzuki, A., Yamaguchi, M.T., Ohteki, T., Sasaki, T., Kaisho, T., Kimura, Y., Yoshida, R., Wakeham, A., Higuchi, T., Fukumoto, M. et al. (2001) T cell-specific loss of Pten leads to defects in central and peripheral tolerance. *Immunity*, **14**, 523–534.
- Di Cristofano, A., Kotsi, P., Peng, Y.F., Cordon-Cardo, C., Elkon, K.B. and Pandolfi, P.P. (1999) Impaired Fas response and autoimmunity in Pten $^{+/-}$ mice. *Science*, **285**, 2122–2125.
- Heindl, M., Händel, N., Ngeow, J., Kionke, J., Wittekind, C., Kamprad, M., Resning-Ehl, A., Ehl, S., Reifenberfer, J., Loddenkemper, C. et al. (2012) Autoimmunity, intestinal lymphoid hyperplasia, and defects in mucosal B-cell homeostasis in patients with PTEN hamartoma tumor syndrome. *Gastroenterology*, **142**, 1093–1096.e6.
- Amer, M., Mostafa, F.F., Attwa, E.M. and Ibrahim, S. (2011) Cowden's syndrome: a clinical, immunological, and histopathological study. *Int. J. Dermatol.*, **50**, 516–521.
- Shrestha, S., Yang, K., Guy, C., Vogel, P., Neale, G. and Chi, H. (2015) Treg cells require the phosphatase PTEN to restrain TH1 and TFH cell responses. *Nat. Immunol.*, **16**, 178–187.
- Eissing, M., Ripken, L., Schreiber, G., Westdorp, H., Ligtenberg, M., Netea-Maier, R., Netea, M.G., de Vries, I.J.M. and Hoogerbrugge, N. (2019) PTEN hamartoma tumor syndrome and immune dysregulation. *Transl. Oncol.*, **12**, 361–367.
- Anderson, M.S., Venanzi, E.S., Klein, L., Chen, Z., Berzins, S.P., Turley, S.J., von Boehmer, H., Bronson, R., Dierich, A., Benoist, C. et al. (2002) Projection of an immunological self shadow within the thymus by the Aire protein. *Science*, **298**, 1395–1401.
- Yanagihara, T., Sanematsu, F., Sato, T., Uruno, T., Duan, X., Tomino, T., Harada, Y., Watanabe, M., Wang, Y., Tanaka, Y. et al. (2015) Intronic regulation of Aire expression by Jmjd6 for self-tolerance induction in the thymus. *Nat. Commun.*, **6**, 8820.
- Yanagihara, T., Tomino, T., Uruno, T. and Fukui, Y. (2017) Thymic epithelial cell-specific deletion of Jmjd6 reduces Aire protein expression and exacerbates disease development in a mouse model of autoimmune diabetes. *Biochem. Biophys. Res. Commun.*, **489**, 8–13.
- Nagamine, K., Peterson, P., Scott, H.S., Kudoh, J., Minoshima, S., Heino, M., Krohn, K.J., Lalot, M.D., Mullis, P.E., Antonarakis, S.E. et al. (1997) Positional cloning of the APECED gene. *Nat. Genet.*, **17**, 393–398.
- Chan, A.Y. and Anderson, M.S. (2015) Central tolerance to self revealed by the autoimmune regulator. *Ann. N. Y. Acad. Sci.*, **1356**, 80–89.
- Shen, W.H., Balajee, A.S., Wang, J., Wu, H., Eng, C., Pandolfi, P.P. and Yin, Y. (2007) Essential role for nuclear PTEN in maintaining chromosomal integrity. *Cell*, **128**, 157–170.
- Chen, Z.H., Zhu, M., Yang, J., Liang, H., He, J., He, S., Wang, P., Kang, X., McNutt, M.A., Yin, Y. et al. (2014) PTEN interacts with histone H1 and controls chromatin condensation. *Cell Rep.*, **8**, 2003–2014.
- Burkly, L., Hession, C., Ogata, L., Reilly, C., Marconi, L.A., Olson, D., Tizard, R., Cate, R. and Lo, D. (1995) Expression of relB is required for the development of thymic medulla and dendritic cells. *Nature*, **373**, 531–536.
- Akiyama, T., Shimo, Y., Yanai, H., Qin, J., Ohshima, D., Maruyama, Y., Asami, Y., Kitazawa, J., Takayanagi, H., Penninger, J.M. et al. (2008) The tumor necrosis factor family receptors RANK and CD40 cooperatively establish the thymic medullary microenvironment and self-tolerance. *Immunity*, **29**, 423–437.
- Li, S., Zhu, M., Pan, R., Fang, T., Cao, Y.-Y., Chen, S., Zhao, X., Lei, C.-Q., Guo, L., Chen, Y. et al. (2016) The tumor suppressor PTEN has a critical role in antiviral innate immunity. *Nat. Immunol.*, **17**, 241–249.
- Garfin, P.M., Nguyen, T. and Sage, J. (2016) Loss of Pten disrupts the thymic epithelium and alters thymic function. *PLoS One*, **11**, e0149430.
- Planchon, S.M., Waite, K.A. and Eng, C. (2008) The nuclear affairs of PTEN. *J. Cell Sci.*, **121**, 249–253.

29. Abbas, A., Padmanabhan, R., Romigh, T. and Eng, C. (2019) PTEN modulates gene transcription by redistributing genome-wide RNA polymerase II occupancy. *Hum. Mol. Genet.*, **28**, 2826–2834.
30. Zhou, Z., Qiu, J., Liu, W., Zhou, Y., Plocinik, R.M., Li, H., Hu, Q., Ghosh, G., Adams, J.A., Rosenfeld, M.G. et al. (2012) The Akt-SRPK-SR axis constitutes a major pathway in transducing EGF signaling to regulate alternative splicing in the nucleus. *Mol. Cell*, **47**, 422–433.
31. Shen, S.-M., Ji, Y., Zhang, C., Dong, S.-S., Yang, S., Xiong, Z., Ge, M.-K., Yu, Y., Guo, M., Cheng, J.-K. et al. (2018) Nuclear PTEN safeguards pre-mRNA splicing to link Golgi apparatus for its tumor suppressive role. *Nat. Commun.*, **9**, 2392.
32. Yi, J., Shen, H.-F., Qiu, J.-S., Huang, M.-F., Zhang, W.-J., Ding, J.-C., Zhu, X.-Y., Zhou, Y., Fu, X.-D., Liu, W. et al. (2017) JMJD6 and U2AF65 co-regulate alternative splicing in both JMJD6 enzymatic activity dependent and independent manner. *Nucleic Acids Res.*, **45**, 3503–3518.
33. Webby, C.J., Wolf, A., Gromak, N., Dreger, M., Kramer, H., Kessler, B., Nielsen, M., Schmitz, C., Butler, D.S., Yates, J.R. et al. (2009) Jmjd6 catalyses lysyl-hydroxylation of U2AF65, a protein associated with RNA splicing. *Science*, **325**, 90–93.
34. Tilot, A.K., Gaugler, M.K., Yu, Q., Romigh, T., Yu, W., Miller, R.H., Frazier, T.W. and Eng, C. (2014) Germline disruption of Pten localization causes enhanced sex-dependent social motivation and increased glial production. *Hum. Mol. Genet.*, **23**, 3212–3227.
35. Lobo, G.P., Waite, K.A., Planchon, S.M., Romigh, T., Nassif, N.T. and Eng, C. (2009) Germline and somatic cancer-associated mutations in the ATP-binding motifs of PTEN influence its subcellular localization and tumor suppressive function. *Hum. Mol. Genet.*, **18**, 2851–2862.
36. He, X., Thacker, S., Romigh, T., Yu, Q., Frazier, T.W. and Eng, C. (2015) Cytoplasm-predominant Pten associates with increased region-specific brain tyrosine hydroxylase and dopamine D2 receptors in mouse model with autistic traits. *Mol. Autism*, **6**, 63.
37. Ruifrok, A.C. and Johnston, D.A. (2001) Quantification of histochemical staining by color deconvolution. *Anal. Quant. Cytol. Histol.*, **23**, 291–299.
38. Varghese, F., Bukhari, A.B., Malhotra, R. and De, A. (2014) IHC profiler: an open source plugin for the quantitative evaluation and automated scoring of immunohistochemistry images of human tissue samples. *PLoS One*, **9**, e96801.